Wagner et al. *EPJ Techniques and Instrumentation* (2023) 10:2
https://doi.org/10.1140/epjti/s40485-023-00090-9
EPJ.org
EPJ Techniques and Instrumentation
RESEARCH ARTICLE
Open Access

Three-dimensional nanowire networks fabricated by ion track nanotechnology and their applications

M.F.P. Wagner[1*], K.-O. Voss[1], C. Trautmann[1,2] and M.E. Toimil-Molares[1*]

*Correspondence:
F.M.Wagner@gsi.de;
m.e.toimilmolares@gsi.de
[1]GSI Helmholtzzentrum für Schwerionenforschung, Darmstadt, Germany
Full list of author information is available at the end of the article

Abstract

The existing and future accelerator facilities at GSI and FAIR offer unique opportunities for interdisciplinary research, especially for material science and nanotechnology. On their way through polymers, swift heavy ions with GeV energy deposit enormous energy densities along their trajectory, generating long nanoscopic damage trails known as ion tracks. Ion-track technology utilizes the small track size (few nm) combined with the extensive track length (up to 100 μm and more) to synthesize and control the geometry of high-aspect-ratio nanostructures such as tailored nanochannels and nanowires. In particular, electrodeposition and ion-track nanotechnology provide an excellent platform for developing unique 3D networks of nanowires with controlled dimensions, composition and crystallographic properties. Here, a summary of recent results obtained on the synthesis and characterization of stable 3D architectures of semiconductor and semimetal nanowires, and their implementation in the fields of photoelectrochemistry and thermoelectrics, is presented.

Keywords: Nanotechnology; Ion tracks; Nanowires; Electroplating; Photoelectrochemistry; Thermoelectricity

1 Introduction

The implementation of nanowires for applications such as thermoelectrics, catalysis, plasmonics, or photoelectrochemical water splitting for hydrogen generation requires both, an excellent control on geometry, crystallinity and composition of the individual nanostructures, as well as the successful assembly into 2D and 3D architectures [1–6]. Fabrication of 3D nanowire superstructures by e.g. vapour–liquid–solid processes has been reported; however, in most cases the tunability of the relevant parameters is limited [7, 8]. Electrodeposition in etched ion-track membranes with interconnected nanochannels, on the other hand, offers high flexibility in the choice of relevant parameters.

Etched ion-track membranes with parallel nanochannels are widely used as templates for the growth of nanowires [3, 9–12]. Their fabrication involves two separate process steps. First, the template material is irradiated with energetic heavy ions creating so-called ion tracks [13]. High energy heavy-ion beams are provided at large accelerator facilities,

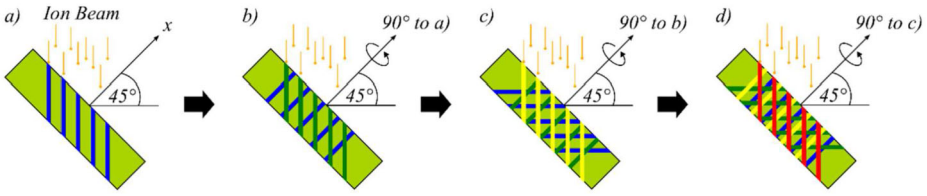

Figure 1 Irradiation scheme for network templates with intersecting pores. The polymer foils are irradiated sequentially from four different directions (**a**)–(**d**) using swift heavy ions. During each irradiation step, the foil is tilted by 45° towards the incoming ion beam. From M.F.P. Wagner, PhD Thesis, Technische Universität Darmstadt, 2018 [1, 4]

such as the universal linear accelerator (UNILAC) of GSI (Darmstadt, Germany). The GSI UNILAC provides heavy ions (up to uranium) of specific energy up to 11.4 MeV/nucleon. Such high energy ion beams have a penetration depth in polymers of about 120 μm, enabling the exposure of foils or stacks of foils with thicknesses between $\sim$ 6 and 100 μm [9]. By chemical etching, the ion tracks are subsequently selectively dissolved and enlarged into open channels. Control over the irradiation and etching conditions enables the production of membranes with channels of predefined geometries, sizes, and aspect ratios. Channel densities can be adjusted between a single channel per polymer foil and $\sim 10^{10}$ cm^{-2} [2, 9, 14–16]. Apart from membranes with parallel channels, novel templates can be obtained by performing the irradiation under several incident angles. Subsequent chemical etching results in templates consisting of a nanochannel network. Electrodeposition in these tilted nanochannels and removal of the polymer matrix leads to freestanding 3-D nanowire networks. A variety of different materials including Pt, Bi, Sb, Cu_2O or ZnO networks have been demonstrated [1–4, 17, 18].

Three dimensional nanowire networks can span over cross-sectional areas of up to several cm^2 with a surface area of up to $\sim$250 cm^2 on a 1 cm^2 planar surface. The junctions between adjacent nanowires render excellent mechanical stability as well as electrical conductivity. The wires mechanically support each other, and in case individual wires break, electrical or thermal transport can still occur via alternative nanowire interconnections [1, 2, 6, 19–21]. By means of several examples, we illustrate how 3D nanowire networks combine the advantages and ease of handling of macroscopic samples with the size-dependent properties of nanowires.

2 Experimental

For the preparation of network templates, stacks of up to 3 polycarbonate foils with a thickness of 30 μm (Makrofol N, Bayer AG) are irradiated at an angle of 45° with respect to the incoming beam. The irradiation is repeated from four different directions, with an angle of 90° between each direction (Fig. 1). The ion species are usually ions of high atomic number such as Au or Bi because of the high energy loss. The specific energy of the ions is 11.1 MeV/nucleon [22].

Prior to chemical etching, the irradiated foils are exposed to UV light using a T-30M Vilber Lourmat lamp (30 W, 312 nm). This process is known to decrease the width of the pore size distribution after etching [23–25]. Selective chemical etching of the ion tracks is performed in 6M NaOH solution at 50 °C yielding cylindrical channels [9, 13, 24]. Under these conditions, the nanochannel diameter grows with a radial rate of 10-12 nm/min

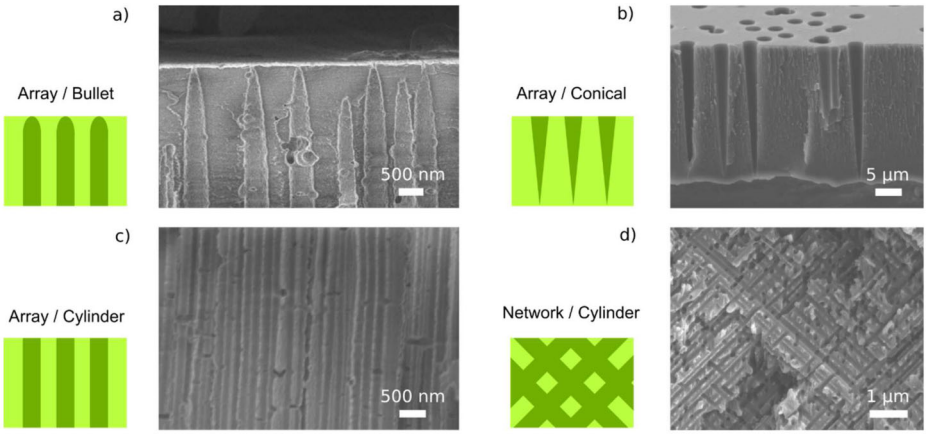

Figure 2 Schematics and scanning electron microscopy images of various pore geometries in ion track-etched membranes illustrating channels with (**a**) asymmetric bullet-like and (**b**) conical shapes, as well as (**c**) symmetric cylindrical parallel and (**d**) interconnected arrangements. Partially adapted from L. Burr, PhD Thesis, Technische Universität Darmstadt, 2017 and L. Movsesyan, PhD Thesis, Technische Universität Darmstadt, 2017

[22]. Figure 2 illustrates various geometries that can be obtained by adjusting geometry and parameters of the etching process. They include channels with asymmetric bullet-like (a) and conical shapes (b), as well as symmetric cylindrical parallel (c) and interconnected (d) arrangements [3, 14–16, 22]. The latter ones are used as templates for the controlled electrodeposition of 3D nanowire networks.

In order to fill the pores by electroplating, first a conductive contact material (e.g. ∼100 nm thin gold layer) is sputtered on one side of the membrane. This initial layer is further reinforced by electroplating a thicker layer usually of gold or copper on top. The conductive layer serves as a working electrode in a three-electrode electrochemical cell during the electrodeposition of the material of choice inside the channels. In most cases, the reaction is controlled via the applied potential (constant or pulsed) in order to avoid the occurrence of side reactions like hydrogen evolution.

The electrodeposition process is monitored by recording the current between the working electrode and a counter electrode as a function of time. The electrodeposition parameters and the employed electrolytes determine the chemical composition, crystallinity, and crystallographic orientation of the resulting nanowires. The length of the nanowires can be adjusted by varying the electrodeposition time. Detailed descriptions of the fabrication processes for the presented materials can be found elsewhere [1, 3, 4, 9, 26, 27].

The 3D nanowire networks are typically characterized by a variety of methods, such as X-ray diffraction (XRD) and scanning or transmission electron microscopy. When direct access to the nanowires is required, the polymer membrane is dissolved in several consecutive baths of dichloro-methane.

3 Photoelectrochemical and thermoelectric applications of nanowire networks

The compact design, mechanical stability, and high surface area of semiconducting 3D nanowire-based networks can be advantageous for specific performances. Here we present two representative examples for applications of 3D nanowire networks.

3.1 ZnO nanowire networks as photoanodes for electrochemical water splitting

Nanowire networks are expected to facilitating efficient light absorption and charge carrier transport in photoelectrodes [3, 5, 28–36]. The one-dimensional geometry and the small diameter of the nanowires is advantageous regarding the transport of charge carriers to the nanowire-electrolyte interface, which in turn should lead to less charge recombination and an increase in photocurrent. Additionally, the large surface to volume ratio generates a large electrode-to-electrolyte interface [3, 33–35]. The network structure here allows for a mechanically rigid and electrically reliable model system for which the various geometrical parameters can be adjusted independently [3, 35].

To investigate the photoelectrochemical performance, a ZnO network was inserted in a photoelectrochemical cell and immersed in a 0.1M K_2SO_4 solution of pH 5.6. A Ag/AgCl (Sat. KCl) electrode served as reference and a Pt-wire as counter electrode. The sample was then illuminated with an arc lamp source with an Xe lamp calibrated at AM 1.5 (1 sun). The illumination generates electron-hole pairs within the material that can be separated by applying a bias voltage. Figure 3 shows the generated photo-current density as a function of the linearly sweeped bias voltage for ZnO nanowire networks and ZnO thin films, while the light was periodically switched off and on. The nanowire networks had a wire density of $\sim 5.7 \times 10^9$ cm^{-2}, wire diameter of $\sim$150 nm and a height of $\sim$30 μm. Here, the potential is reported versus the reversible hydrogen electrode according to:

$$E_{\mathrm{RHE}} = E_{\mathrm{Ag/AgCl}} + 0.059\, pH + E^0_{\mathrm{Ag/AgCl}}.$$

For both cases, also samples with a 20 nm thick TiO_2 layer, that was applied by atomic layer deposition are shown. The TiO_2 layer was applied to protect ZnO versus photocorrosion as can be seen in Fig. 4. In general, the networks show a larger photocurrent than flat films. The films exhibit relatively constant photocurrent densities of 0.02 mA/cm^2 and 0.06 mA/cm^2 for at 1.5 V vs. RHE with and without additional TiO_2, respectively, whereas the networks generated 0.1 mA/cm^2 and 0.35 mA/cm^2 that were increasing with increasing bias voltage. The fivefold increase in the current generated by the networks was attributed to the geometrical advantages explained above. The higher performance of the TiO_2 coated samples is ascribed to additional electron-hole pairs generated within the TiO_2 layer and additional contributions to the charge carrier separation by the ZnO-TiO_2 interface, which further helps to reduce the probability of charge carrier recombination [37, 38].

Additional experiments were performed on networks covered with 20 nm TiO_2 with a lower nanowire number density of 1.4×10^9 cm^{-2} and various nanowire diameters, shown in Fig. 5. Here, the larger the nanowire diameter the denser the network and, correspondingly, the higher the generated photocurrents. This is attributed to a larger amount of photoactive material in the denser networks. Also the variation of the photocurrents as a function of the applied bias voltage increases with increasing nanowire diameter. In all cases the generated photocurrents of the networks were higher than the corresponding reference value for the thin films. These measurements demonstrate that nanowire networks are most suitable model systems and enables a systematic investigation of the geometrical factors influencing photoelectrochemical water splitting. Similar results were obtained for Cu_2O nanowire-based photocathodes [17].

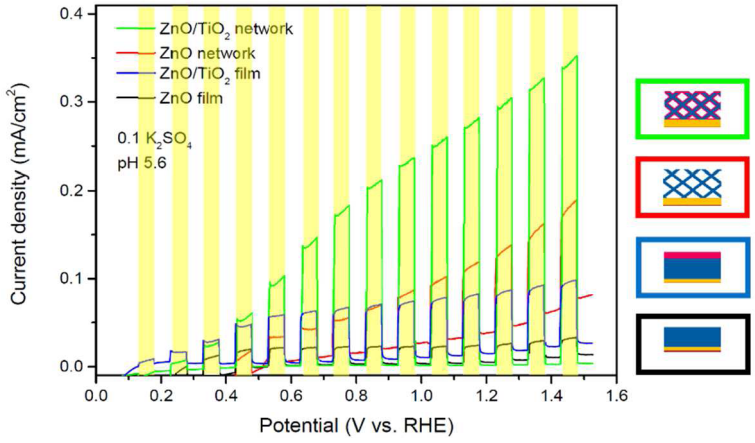

Figure 3 Measured generated photocurrents for ZnO nanowire networks and ZnO films with and without a TiO_2 protection layer during a linear bias voltage sweep. Yellow areas mark when the samples were illuminated, white areas when the light was switched off. From L. Movsesyan et al., ©Nanomaterials 8, 693 (2018)

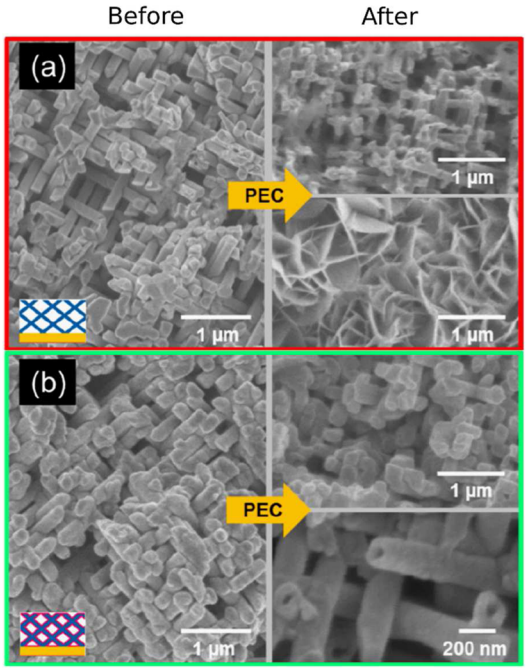

Figure 4 SEM images of ZnO nanowire networks with and without a TiO_2 protection layer after photoelectrochemical experiments. (**a**) After one hour of reaction, the nanowires decay and recrystallization of ZnO occurs. (**b**) After three hours of photocorrosion, the network coated with TiO_2 shows no or only small corrosion effects. From L. Movsesyan et al., ©Nanomaterials 8, 693 (2018)

3.2 Bi and Sb nanowire networks for thermoelectric applications

The dimensionless thermoelectric figure-of-merit $Z \cdot T = S^2 \cdot \sigma \cdot T/(\lambda_{el} + \lambda_{ph})$ describes the efficiency of the material for thermoelectric applications [39–41]. Here, S is the Seebeck coefficient, σ is the electrical conductivity and λ_{el}, λ_{ph} are the respective thermal conductivities by charge carriers and phonons of a given material. The interdependency of S, σ,

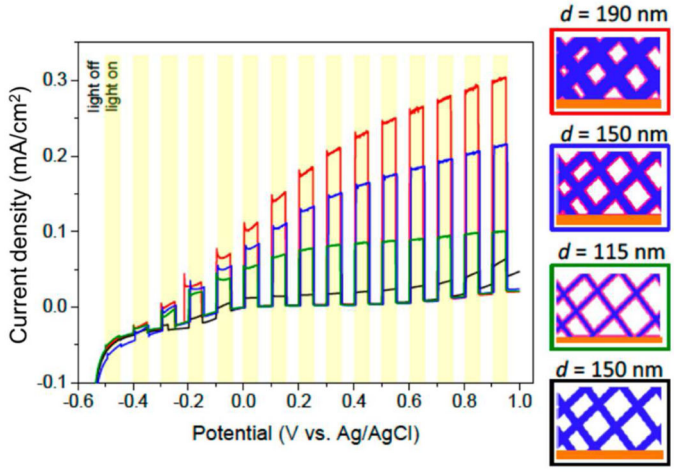

Figure 5 Photocurrents for uncoated and TiO_2-coated ZnO nanowire networks with different wire diameters during a linear bias voltage sweep. Yellow and white areas correspond to illuminated or dark samples, respectively. From L. Movsesyan et al., ©Nanomaterials 8, 693 (2018)

and λ_{el} via the charge carrier density hinders the increase of ZT. Commercial thermoelectric materials nowadays exhibit maximal ZT values of ∼1 [40, 42–44]. However, for widespread applications of thermoelectric modules a ZT of 3 would be required [45–47].

The size effects expected in small nanowires can help to decouple the electrical and thermal transport and thereby open up a route for further improvement of thermoelectric materials [43, 44, 48]. $Bi_{(1-x)}Sb_x$ bulk has already been proven suitable for thermoelectric applications at low temperatures [40]. The material system is also ideal for studying the influence of size effects on transport and thermoelectrical properties, because the mean free paths of charge carriers and phonons in Bi and Sb at room temperature are in the order of 100 nm, and the Fermi wavelength in the order of 40 nm [40, 43, 48–53]. Size effects therefore already occur at relatively large dimensions. Potentially, nanowire arrays exhibiting higher ZT values will yield more efficient thermocouples, which are of great interest for infrared sensor applications [54]. Crossplane relative electrical resistivity and Seebeck coefficient of Sb nanowire networks as a function of temperature were investigated using a custom-build setup described elsewhere [1, 55, 56]. Figure 6 shows the relative electrical resistance and Seebeck coefficient of Sb nanowire networks with $\sim 1.4 \times 10^9$ wires·cm^{-2} and wire diameters ranging between 30 to 140 nm as a function of temperature. In all samples, the relative electrical resistance exhibits a metallic behaviour. The electrical resistivity of the nanowire networks with smaller wire diameters is dominated by scattering of charge carriers at the nanowire surface and on grain boundaries, as theoretically described by Mayadas, Shatzkes, Fuchs, Sondheimer and Dingle, for both thin films and nanowires [57–60]. Therefore, with decreasing wire diameter, the electrical resistance is less affected by a decrease in temperature and the corresponding increase in mean free path of the charge carriers. The measured Seebeck coefficient for the Sb networks is in the order of 20 – 25 μV/K. Bulk Sb is very anisotropic and has a maximal Seebeck coefficient of ∼47 μV/K for transport along the binary axis [40]. According to XRD measurements, the Sb networks exhibited a {01.2} texture, while also the {10.4} and {11.0} planes were observed [22]. Due to this, the Seebeck coefficient is smaller than ∼47 μV/K, but comparable to the Seebeck

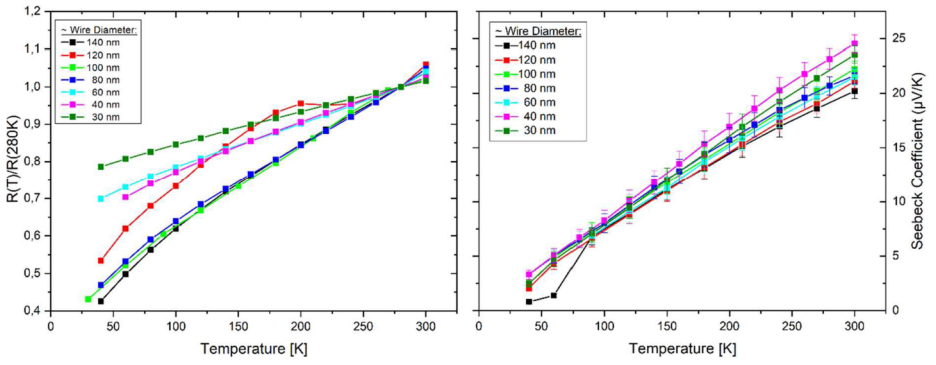

Figure 6 Relative electrical resistance and Seebeck coefficient of Sb nanowire networks with a nanwire density of 1.4×10^9 cm^{-2} and various wire diameters as a function of temperature. From M.F.P. Wagner, PhD Thesis, Technische Universität Darmstadt, 2018

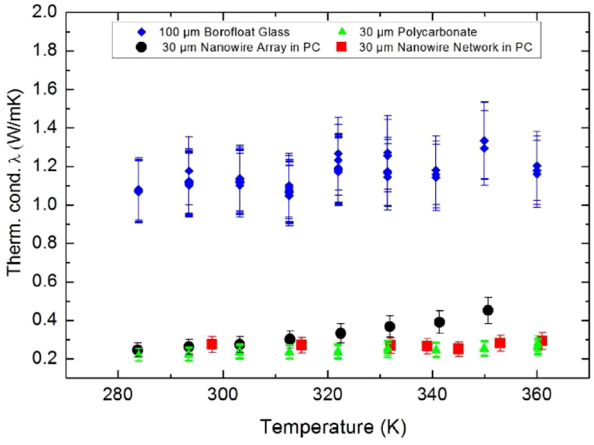

Figure 7 Thermal conductivity of various samples as a function of temperature. From M.F.P. Wagner, PhD Thesis, Technische Universität Darmstadt, 2018

coefficient of Sb bulk for other crystal orientations. The nanowire networks with smallest diameters have a slightly higher Seebeck coefficient at room temperature, possibly because of small variations in crystallinity for the different wire diameters [61–63]. With decreasing temperature, the values monotonously decrease towards zero, as expected [39, 40]. Figure 7 shows the thermal conductivities of the polycarbonate template material as well as Sb nanowire arrays and nanowire networks measured using a method described elsewhere [4]. As comparison, also the well-known thermal conductivity of a Borofloat glass was measured. The thermal conductivity measured for nanowire networks and nanowire arrays (∼0.3–0.4 W/mK) is significantly smaller than for bulk Sb (λ = 24 W/mK), which is attributed to enhanced phonon scattering at the nanowire's surfaces [20, 21, 40, 64]. Since the Seebeck coefficient is similar to bulk and thermal conductivity is significantly suppressed, the thermoelectric efficiency ZT is most probably increased for the networks compared to bulk material, making nanowire networks promising materials for thermoelectric applications. To demonstrate this, absolute values of the electrical resistance have to be measured in the future.

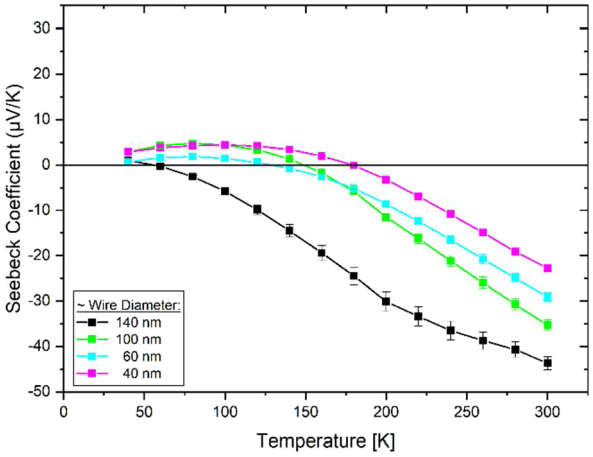

Figure 8 Seebeck coefficient of Bi nanowire networks with a wire density of 1.4×10^9 cm^{-2} as a function of temperature. From M.F.P. Wagner, PhD Thesis, Technische Universität Darmstadt, 2018

Figure 8 shows the Seebeck coefficient of Bi nanowire networks with different wire diameters as a function of temperature. The Seebeck coefficients at room temperature are similar to previously reported values for nanowires and are comparable to theoretical values assigned to the bisectrix axis in Bi nanowires [48, 65]. The Seebeck coefficient measured at room temperature decreases with decreasing nanowire diameter, due to the limitation of the mean free path of the charge carriers, and possibly also due to the influence of surface states which is more important for higher surface-to-volume ratios [56, 65–67]. With decreasing temperature, the Seebeck coefficient decreases, exhibiting a change of sign which was not observed in the case of Sb nanowires. The data show that the temperature at which the sign change occurs depends on the diameter of the nanowires, namely the temperature shifts to higher values with decreasing nanowire diameter. A similar behaviour was theoretically predicted by Murata et al. for Bi nanowires with crystals oriented along the bisectrix axis [67]. According to Murata et al., this sign change can be attributed to a different dependence of hole and electron mobility on nanowire diameter and temperature. In semimetals, the Seebeck coefficient S is made up of contributions of holes and electrons according to $S = (S_n\sigma_n + S_p\sigma_p)/(\sigma_n + \sigma_p)$, where $S_{n,p}$ and $\sigma_{n,p}$ are the Seebeck coefficient and electrical conductivity of electrons and holes, respectively [40]. Under the assumption that both charge carrier densities are similar, this means that at the transition temperature, the mobility of holes becomes larger than the one of electrons [65]. At small dimensions also topological surface states can additionally contribute to transport [56, 66, 67]. As the properties of topological transport in bismuth and antimony are still under discussion, further transport measurements will unravel new and exciting effects on the transport behavior of tailored Bi and Sb nanostructures [68].

4 Conclusion

Selected examples illustrate how macroscopic, cm-sized samples with three-dimensional nanowire networks exhibit size-dependent properties. Such well-defined tailored networks are excellent candidates to serve as tailored model systems to elucidate the influence of surface, size and geometry factors. Optimized nanosystems are required for novel

devices in many different fields including thermoelectrics, photoelectrochemistry, sensing, or catalysis. The combination of ion-track nanotechnology and electroplating yields nanowire networks of a large variety of technological relevant materials, while providing excellent control on their chemical, structural and morphological properties. The large number of well-defined interconnections between adjacent nanowires provides excellent electrical connectivity and gives the samples a remarkable mechanical stability even without a supporting matrix.

Acknowledgements
Research activities on Bi and Sb nanowires are part of the Helmholtz Innovation Pool Project "MadQuanT". The nanowire samples were produced based on UMAT irradiations performed at the beam line X0 at the GSI Helmholtzzentrum für Schwerionenforschung, Darmstadt (Germany) in the frame of FAIR Phase-0. The publication is funded by the Deutsche Forschungsgemeinschaft (DFG, German Research Foundation)—491382106, and by the Open Access Publishing Fund of GSI Helmholtzzentrum fuer Schwerionenforschung.

Funding
GSI Helmholtzzentrum für Schwerionenforschung, Darmstadt (Germany). Open Access funding enabled and organized by Projekt DEAL.

Availability of data and materials
The data that support the findings in this study are available from the corresponding author upon reasonable request.

Declarations

Competing interests
The authors have no competing interests to disclose.

Author contribution
MFPW was a major contributor in writing the manuscript and performed the measurements, analysis and interpretation of data in Sect. 3.2. K-OV contributed to the experimental design and created the programs for data acquisition in Sect. 3.2 and contributed in analysis and interpretation of the acquired data. CT has made substantial contribution to the experimental design, analysis and interpretation of the acquired data and contributed in writing the manuscript. MET-M has made substantial contribution to the experimental design, analysis and interpretation of the acquired data and was a major contributor in writing the manuscript. All authors read and approved the final manuscript.

Author details
[1]GSI Helmholtzzentrum für Schwerionenforschung, Darmstadt, Germany. [2]Technische Universität Darmstadt, Darmstadt, Germany.

Publisher's Note

Received: 8 November 2022 Accepted: 18 January 2023 Published online: 22 February 2023

References

1. Wagner MFP et al. Effects of size reduction on the electrical transport properties of 3D Bi nanowire networks. Adv Electron Mater. 2021;7:2001069.
2. Rauber M et al. Highly-ordered supportless three-dimensional nanowire networks with tunable complexity and interwire connectivity for device integration. Nano Lett. 2011;11:2304–10.
3. Movsesyan L et al. ZnO nanowire networks as photoanode model systems for photoelectrochemical applications. Nanomaterials. 2018;8:693.
4. Wagner MFP, Völklein F, Reith H, Trautmann C, Toimil-Molares ME. Fabrication and thermoelectrical characterization of three-dimensional nanowire networks. Phys Status Solidi. 2016;213:610–9.
5. Ponzoni A et al. Ultrasensitive and highly selective gas sensors using three-dimensional tungsten oxide nanowire networks. Appl Phys Lett. 2006;88:203101.
6. Huber TE, Graf MJ. Electronic transport in a three-dimensional network of one-dimensional bismuth quantum wires. Phys Rev B. 1999;60:16880–4.
7. Norris KJ et al. Indium phosphide nanowire network: growth and characterization for thermoelectric conversion. In: Kobayashi NP, Talin AA, Islam MS, editors. Proceedings volume 8467, nanoepitaxy: materials and devices IV. vol. 84670E. 2012. https://doi.org/10.1117/12.929861.
8. Stanley SA, Stuttle C, Caruana AJ, Cropper MD, Walton ASO. An investigation of the growth of bismuth whiskers and nanowires during physical vapour deposition. J Phys D, Appl Phys. 2012;45:435304.
9. Toimil-Molares ME. Characterization and properties of micro- and nanowires of controlled size, composition, and geometry fabricated by electrodeposition and ion-track technology. Beilstein J Nanotechnol. 2012;3:860–83.

10. Cassinelli M. Thermoelectric properties of Bi1-xSbx nanowires electrodeposited in etched ion-track membranes. Darmstadt: Technische Universität Darmstadt; 2016.
11. Krieg J. Characterization of individual Bi2Te3 nanowires electrodeposited in etched ion-track membranes for nano-ARPES and electrical transport studies. Darmstadt: TU; 2017.
12. Müller S et al. Electrochemical synthesis of Bi 1– x Sb x nanowires with simultaneous control on size, composition, and surface roughness. Cryst Growth Des. 2012;12:615–21.
13. Trautmann C. Observation and chemical treatment of heavy-ion tracks in polymers. Nucl Instrum Methods Phys Res, Sect B, Beam Interact Mater Atoms. 1995;105:81–5.
14. Lee PLJ et al. Etched ion-track membranes as tailored separators in Li–S batteries. Nanotechnology. 2021;32:365401.
15. Ulrich N et al. Conical nanotubes synthesized by atomic layer deposition of Al2O3, TiO2, and SiO2 in etched ion-track nanochannels. Nanomaterials. 2021;11:1874.
16. Laucirica G et al. Shape matters: enhanced osmotic energy harvesting in bullet-shaped nanochannels. Nano Energy. 2020;71:104612.
17. Yang F et al. Cu 2 O/TiO 2 nanowire assemblies as photocathodes for solar hydrogen evolution: influence of diameter, length and NumberDensity of wires. Z Phys Chem. 2020;234:1205–21.
18. Caddeo F et al. Tuning the size and shape of NanoMOFs via templated electrodeposition and subsequent electrochemical oxidation. ACS Appl Mater Interfaces. 2019;11:25378–87.
19. Pennelli G, Totaro M, Piotto M, Bruschi P. Seebeck coefficient of nanowires interconnected into large area networks. Nano Lett. 2013;13:2592–7.
20. Verdier M, Lacroix D, Termentzidis K. Thermal transport in two- and three-dimensional nanowire networks. Phys Rev B. 2018;98:155434.
21. Roslyak O, Piryatinski A. Thermoelectric properties of semiconductor nanowire networks. J Appl Phys. 2016;119:125107.
22. Wagner MFP. Bi and Sb nanowire assemblies for thermoelectric applications. Darmstadt: Technische Universität; 2018.
23. Cornelius TW et al. Nanopores in track-etched polymer membranes characterized by small-angle x-ray scattering. Nanotechnology. 2010;21:155702.
24. Pépy G et al. Cylindrical nanochannels in ion-track polycarbonate membranes studied by small-angle X-ray scattering. J Appl Crystallogr. 2007;40:s388–92.
25. Ferain E, Legras R. Heavy ion tracks in polycarbonate. Comparison with a heavy ion irradiated model compound (diphenyl carbonate). Nucl Instrum Methods Phys Res, Sect B, Beam Interact Mater Atoms. 1993;82:539–48.
26. Movsesyan L, Schubert I, Yeranyan L, Trautmann C, Eugenia Toimil-Molares M. Influence of electrodeposition parameters on the structure and morphology of ZnO nanowire arrays and networks synthesized in etched ion-track membranes. Semicond Sci Technol. 2016;31:014006.
27. Wagner MFP. Bi and Sb nanowire assemblies for thermoelectric applications. 2018.
28. Alenezi MR, Henley SJ, Emerson NG, Silva SRP. From 1D and 2D ZnO nanostructures to 3D hierarchical structures with enhanced gas sensing properties. Nanoscale. 2014;6:235–47.
29. Liu R, Duay J, Lee SB. Heterogeneous nanostructured electrode materials for electrochemical energy storage. Chem Commun. 2011;47:1384–404.
30. Duay J, Gillette E, Hu J, Lee SB. Controlled electrochemical deposition and transformation of hetero-nanoarchitectured electrodes for energy storage. Phys Chem Chem Phys. 2013;15:7976.
31. Wei D et al. A nanostructured electrochromic supercapacitor. Nano Lett. 2012;12:1857–62.
32. Hochbaum AI, Yang P. Semiconductor nanowires for energy conversion. Chem Rev. 2010;110:527–46.
33. Zhong M, Ma Y, Oleynikov P, Domen K, Delaunay J-J. A conductive ZnO–ZnGaON nanowire-array-on-a-film photoanode for stable and efficient sunlight water splitting. Energy Environ Sci. 2014;7:1693.
34. van de Krol R, Liang Y, Schoonman J. Solar hydrogen production with nanostructured metal oxides. J Mater Chem. 2008;18:2311.
35. Shi J, Hara Y, Sun C, Anderson MA, Wang X. Three-dimensional high-density hierarchical nanowire architecture for high-performance photoelectrochemical electrodes. Nano Lett. 2011;11:3413–9.
36. Wang Y et al. Fully solar-powered photoelectrochemical conversion for simultaneous energy storage and chemical sensing. Nano Lett. 2014;14:3668–73.
37. Liu M, Nam C-Y, Black CT, Kamcev J, Zhang L. Enhancing water splitting activity and chemical stability of zinc oxide nanowire photoanodes with ultrathin titania shells. J Phys Chem C. 2013;117:13396–402.
38. Hu S et al. Amorphous TiO 2 coatings stabilize Si, GaAs, and GaP photoanodes for efficient water oxidation. Science. 2014;344:1005–9.
39. Goldsmid HJ. Introduction to thermoelectricity. Berlin: Springer; 2010. https://doi.org/10.1007/978-3-642-00716-3.
40. *Thermoelectrics Handbook*. *Thermoelectrics Handbook*. CRC Press; 2006
41. Vedernikov MV, Iordanishvili EK. A.F. Ioffe and origin of modern semiconductor thermoelectric energy conversion. In: Int. conf. Thermoelectr. ICT, proc. New York IEEE Press; 1998. p. 37–42. https://doi.org/10.1109/ICT.1998.740313.
42. Szczech JR, Higgins JM, Jin S. Enhancement of the thermoelectric properties in nanoscale and nanostructured materials. J Mater Chem. 2011;21:4037–55.
43. Heremans JP. Low-dimensional thermoelectricity. Acta Phys Pol A. 2005;108:609–34.
44. Cornett JE, Rabin O. Thermoelectric figure of merit calculations for semiconducting nanowires. Appl Phys Lett. 2011;98:182104.
45. Bell LE. Cooling heating generating power, and recovering waste heat with thermoelectric systems. Science. 2008;321:1457–61.
46. DiSalvo FJ. Thermoelectric cooling and power generation. Science. 1999;285:703–6.
47. Casati G, Mejía-Monasterio C, Prosen T. Increasing thermoelectric efficiency: a dynamical systems approach. Phys Rev Lett. 2008;101:016601.
48. Kim J, Shim W, Lee W. Bismuth nanowire thermoelectrics. J Mater Chem C. 2015;3:11999–2013.
49. Lin Y-M, Cronin SB, Ying JY, Dresselhaus MS, Heremans JP. Transport properties of Bi nanowire arrays. Appl Phys Lett. 2000;76:3944–6.
50. Heremans J, Thrush CM. Thermoelectric power of bismuth nanowires. Phys Rev B. 1999;59:12579–83.

51. Cornelius TW, Toimil-Molares ME. Finite- and Quantum-size effects of bismuth nanowires. In: Nanowires. InTech, 2010. https://doi.org/10.5772/39516.
52. Yang FY et al. Large magnetoresistance of electrodeposited single-crystal bismuth thin films. Science. 1999;284:1335–7.
53. Molares MET et al. Fabrication and contacting of single Bi nanowires. Nanotechnology. 2004;15:S201–7.
54. Lindeberg M, Yousef H, Rödjegård H, Martin H, Hjort K. A PCB-like process for vertically configured thermopiles. J Micromech Microeng. 2008;18:065021.
55. Mueller S. Morphological, Structural, and Compositional Characterization of Electrodeposited Bi1-xSbx Nanowires. Ruprecht–Karls–Universität Heidelberg; 2012
56. Cassinelli M et al. Influence of surface states and size effects on the Seebeck coefficient and electrical resistance of Bi 1-x Sb x nanowire arrays. Nanoscale. 2017;9:3169–79.
57. Mayadas AF, Shatzkes M. Electrical-resistivity model for polycrystalline films: the case of arbitrary reflection at external surfaces. Phys Rev B. 1970;1:1382–9.
58. Dingle RB. The electrical conductivity of thin wires. Proc R Soc Lond Ser A, Math Phys Sci. 1950;201:545–60.
59. Fuchs K. The conductivity of thin metallic films according to the electron theory of metals. Math Proc Camb Philos Soc. 1938;34:100–8.
60. Sondheimer EH. The mean free path of electrons in metals. Adv Phys. 1952;1:1–42.
61. Picht O et al. Tuning the geometrical and crystallographic characteristics of Bi 2 Te 3 nanowires by electrodeposition in ion-track membranes. J Phys Chem C. 2012;116:5367–75.
62. Karim S et al. Synthesis of gold nanowires with controlled crystallographic characteristics. Appl Phys A. 2006;84:403–7.
63. Liu J et al. Electrochemical fabrication of single-crystalline and polycrystalline Au nanowires: the influence of deposition parameters. Nanotechnology. 2006;17:1922–6.
64. Hochbaum AI et al. Enhanced thermoelectric performance of rough silicon nanowires. Nature. 2008;451:163–7.
65. Murata M, Yamamoto A, Hasegawa Y, Komine T, Endo A. Theoretical modeling of electrical resistivity and Seebeck coefficient of bismuth nanowires by considering carrier mean free path limitation. J Appl Phys. 2017;121:014303.
66. Shin HS et al. The surface-to-volume ratio: a key parameter in the thermoelectric transport of topological insulator Bi 2 Se 3 nanowires †. Nanoscale. 2016;8:13552–7.
67. Gooth J et al. Thermoelectric performance of classical topological insulator nanowires. Semicond Sci Technol. 2015;30:015015.
68. Schindler F et al. Higher-order topology in bismuth. Nat Phys. 2018;14:918–24.